PAPER

Check for updates

Concentration dependence of resistance components in solutions containing dissolved Fe²⁺/Fe³⁺

Dai Inoue[a] and Yutaka Moritomo [ID] *[abc]

Electrolyte solutions containing Fe^{2+}/Fe^{3+} are suitable for liquid thermoelectric conversion devices (LTEs), because they are inexpensive materials and exhibit a high electrochemical Seebeck coefficient α. Here, we investigated the concentration (c) dependence of resistance components, *i.e.*, solvent (R_s), charge-transfer (R_{ct}), and diffusion (R_{dif}) resistances, of dissolved-Fe^{2+}/Fe^{3+}-containing aqueous, methanol (MeOH), acetone, and propylene carbonate (PC) solutions. We found that the c dependence of R_s and R_{dif} are well reproduced by empirical formulas, $R_s^{-1} = C_s \dfrac{c}{\eta(c)}$ and $R_{dif}^{-1} = C_{dif} \dfrac{c}{\eta(c)^{1/2}}$, where $\eta(c)$ is viscosity at c.

We further found that the magnitudes of C_s and C_{dif} are nearly independent of solvent, suggesting that η is one of the significant solution parameters that determine R_s and R_{dif}.

1 Introduction

Energy-harvesting devices are attracting the current attention of researchers from the viewpoint of a basic power source for the internet of things (IoT) society as well as sustainable development goals (SDGs). Thermoelectric conversion devices (TEs) are promising because they cover the field from bioelectric and wearable electronics to industrial power generation. In particular, flexible TEs using cellulose gel[1] have excellent compatibility with various thermoelectric conversion materials. This is because cellulose can be used in the design of flexible and ion/electron conductive materials with robust mechanical properties. Flexible TEs are expected to be used not only for thermoelectric conversion but also for sensors and refrigeration units.

Among TEs, liquid thermoelectric conversion devices (LTEs) are promising because they are made of inexpensive materials. There is already a long history of LTE research.[2] Nevertheless, vigorous research has become more active in recent years and many research results have been reported.[3–19] The performance of LTEs is governed by the electrochemical Seebeck coefficient α, effective electric conductivity σ, and effective thermal conductivity κ of the electrolyte.[20] Unlike solid thermoelectric devices, σ is related to the charge transfer and diffusion processes of redox ions as well as the conventional ion migration. The magnitude of σ depends on the microscopic structure

[a]Graduate School of Pure & Applied Science, University of Tsukuba, Tennodai 1-1-1, Tsukuba, Ibaraki 305-8571, Japan. E-mail: moritomo.yutaka.gf@u.tsukba.ac.jp

[b]Faculty of Pure & Applied Science, University of Tsukuba, Tennodai 1-1-1, Tsukuba, Ibaraki 305-8571, Japan

[c]Tsukuba Research Center for Energy Materials Science (TREMS), University of Tsukuba, Tsukuba, Ibaraki 305-8571, Japan

and material of the electrodes.[16,17] In addition, effective σ and κ are influenced by convection of the electrolyte induced by ΔT. The dimensionless figure of merit ($ZT = \dfrac{\alpha^2 \sigma T}{\kappa}$, where T is temperature) is a measure of the LTE performance. With the increase of ZT, the thermal efficiency η increases toward the Carnot efficiency $\left(= \dfrac{\Delta T}{T_H} \right)$, which is the maximum efficiency of a heat engine.[21] To enhance ZT, it is effective to increase (decrease) α and σ (κ).

In recent years, research on LTEs using an organic electrolyte[18,19] has begun to attract attention, as has research on conventional LTEs using an aqueous electrolyte.[4–17] This is because the organic electrolytes exhibit both large α and small κ. In several organic solutions containing Fe^{2+}/Fe^{3+}, α is higher than the value ($= 1.4$ mV K⁻¹) of an aqueous solution. For example, α is 3.6 mV K⁻¹ in acetone solution and 1.8 mV K⁻¹ in propylene carbonate (PC) solution.[22] In addition, κ of a typical organic solvent is ≈ 0.2 W K⁻¹ m⁻¹ and is approximately 33% of the value ($= 0.6$ W K⁻¹ m⁻¹) of water. Recently, Wake *et al.*[18,19] showed that LTEs composed of dissolved-Fe^{2+}/Fe^{3+}-containing methanol (MeOH) and acetone solutions exhibit a large power factor (PF $= \alpha^2 \sigma$) comparable to that of the corresponding aqueous LTE. They also reported α and σ against solute concentration c. The disadvantage of organic electrolytes is a small σ value compared with that of an aqueous electrolyte. Except for aqueous electrolyte,[7] there exists no detailed investigation on the resistance components. Therefore, the origin of the small σ in organic electrolytes is still unclear. Here, we will investigate the resistance components of several solutions containing dissolved Fe^{2+}/Fe^{3+} against c to deeply understand σ and to obtain guidelines for increasing σ in organic electrolytes.

In general, the resistance R ($= \frac{d}{s\sigma}$, where d and s are the electrode distance and area, respectively) of an electrolyte solution consists of the solution resistance R_s due to ion migration, charge transfer resistance R_{ct} due to electron transfer, and diffusion resistance R_{dif} due to reactant/product diffusion.[23] Among them, R_s is derived from the balance between the electric force ($=|z|eE_{ef}$; $|z|$, e, and E_{ef} are the charge number, elementary charge, and electric field, respectively) and frictional force. According to Stokes' law, the latter force is expressed as $6\pi\eta rv$, where η, r, and v are the viscosity, effective radius, and velocity of the ion, respectively. Then, the mobility u $\left(\equiv \frac{v}{E_{ef}}\right)$ of an ion is expressed as $u = \frac{|z|e}{6\pi\eta r}$ and is inversely proportional to η. On the other hand, R_{ct} and R_{dif} are governed by the reaction kinetics in the vicinity of the electrode surface and are independent of d. The reaction rate k is expressed as $k \propto \exp\left(-\frac{e\Delta E}{k_B T}\right)$, where ΔE ($= E - E_{eq}$; E and E_{eq} are the electrode and equilibrium potentials, respectively) and k_B are the overpotential and Boltzmann constant, respectively. In the region of $\Delta E \ll \frac{k_B T}{e}$, the charge-transfer current J_{ct} is expressed as $J_{ct} = \frac{i_0 e}{k_B T}\Delta E$,[23] where i_0 is the exchange current. Thus, R_{ct} is proportional to $\frac{k_B T}{i_0 e}$ and is independent of d. The physical meaning of R_{dif} is as follows. As the reaction progresses, the concentration of reactants/products at the electrode surface changes in a way that prevents further reaction. For the reaction to continue, the reactants/products must diffuse into/from the bulk region. Note that the diffusion current of reactants/products is driven by the concentration gradient created by the reaction at the electrode surface and is independent of d.

In this work, we investigated the c-dependence of R_s, R_{ct}, and R_{dif} of dissolved-Fe^{2+}/Fe^{3+}-containing aqueous, MeOH, acetone, and PC solutions. We found that the c-dependence of R_s and R_{dif} is well reproduced by empirical formulas, $R_s^{-1} = C_s \frac{c}{\eta(c)}$ and $R_{dif}^{-1} = C_{dif} \frac{c}{\eta(c)^{1/2}}$. We further found that their coefficients, C_s and C_{dif}, are nearly independent of solvent, suggesting that η is one of the significant solution parameters that determine R_s and R_{dif}.

2 Experimental methods

2.1 Solution preparation

In this study, water, MeOH, acetone, and PC were selected as the solvents because they exhibit a high solubility of $Fe(ClO_4)_2/Fe(ClO_4)_3$. We prepared aqueous, MeOH, acetone, and PC solutions containing c M $Fe(ClO_4)_2 \cdot 6.0H_2O$ and c M $Fe(ClO_4)_3 \cdot 7.1H_2O$. Distilled water, MeOH, acetone, PC, and solutes were purchased from FUJIFILM Wako Corp. and used as received. Table 1 shows the solubility s and critical concentration c^* of $Fe(ClO_4)_2/Fe(ClO_4)_3$ in the four solvents. c^* is defined as the

Table 1 Solubility s and critical concentration c^* of $Fe(ClO_4)_2 \cdot 6.0H_2O/Fe(ClO_4)_3 \cdot 7.1H_2O$ in several solvents at 298 K. c^* is defined as the concentration at which one Fe ion is dissolved per six solvent molecules. MeOH and PC represent methanol and propylene carbonate, respectively

Solvent	s (M)	c^* (M)
Water	2.5	4.62
MeOH	2.5	2.06
Acetone	1.2	1.12
PC	1.5	0.97

concentration at which one Fe ion is dissolved per six solvent molecules. At $c = c^*$, all solvent molecules are on average coordinated with Fe ions.

2.2 Total resistance

The total resistance R_{tot} of the electrolyte was measured in a two-pole cell at 298 K.[24] The electrodes were produced from a 220 μm graphite sheet (PREMA-FOIL, TOYO TANSO). The electrode distance d and area s are 1.0 cm and 0.42 cm², respectively. The voltage drop V was measured against the current I ($I \leq 0.4$ mA) with a multimeter. I was changed in a stepwise manner at intervals of several minutes. V was stable and no change over time was observed. The slope of the I–V plot corresponds to R_{tot}.

2.3 Electrochemical impedance spectroscopy

R_{ct} and R_{dif} were evaluated in the same cell with the same electrodes. d and s are 1.0 cm and 0.42 cm², respectively. Electrochemical impedance spectroscopy (EIS) was performed at 298 K with use of a potentiostat (Vertex.one.EIS, Ivium Technologies). The frequency range was from 50 mHz to 100 kHz, and the amplitude was 10 mV. V was stable and no change over time was observed. It was confirmed that almost identical EIS data were obtained through multiple measurements.

The EIS data were analyzed with a Randles equivalent circuit,[23] which consists of R_s, R_{ct}, double layer capacitance C_d, and Warburg impedance Z_ω. Z_ω is expressed as $Z_\omega = A_W(\omega^{-1/2} - i\omega^{-1/2})$, where A_W and ω are the Warburg coefficient and angular velocity, respectively. It was difficult to evaluate the magnitude of R_{dif} from A_W even though Z_ω describes the diffusion process of the reactants/products. In the present study, we tentatively evaluate the R_{dif} values by subtraction of R_s and R_{ct} from R_{tot}. We confirmed a positive correlation between A_W and R_{dif} ($= R_{tot} - R_s - R_{ct}$), which strongly supports the correctness of our evaluation method of R_{dif} (*vide infra*).

3 Results

3.1 Total resistance

Fig. 1 shows examples of the I–V plot of several solutions containing dissolved Fe^{2+}/Fe^{3+} at 298 K: (a) water, (b) MeOH, (c) acetone, and (d) PC. For all solutions, V increases in proportion to I. R_{tot} was evaluated from the slope of the plots, as indicated by the straight lines. The obtained R_{tot} values are listed in Table
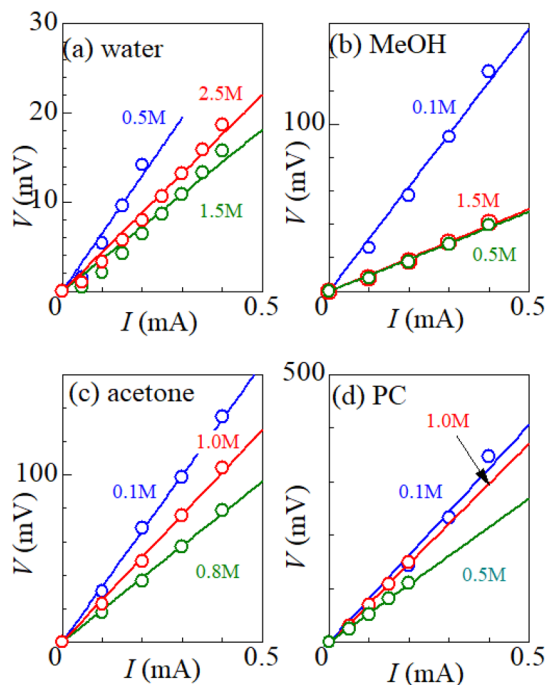
Fig. 1 Voltage V against current I for several solutions containing dissolved Fe^{2+}/Fe^{3+} at 298 K: (a) water, (b) MeOH, (c) acetone, and (d) PC. Data for three typical solute concentrations are shown for each solution: below the resistance minimum (blue), near the resistance minimum (green), and above the resistance minimum (red). The straight lines are the results of least-squares fits.

Table 2 Total resistance R_{tot}, solution resistance R_s, charge-transfer resistance R_{ct}, diffusion resistance R_{dif}, and Warburg coefficient A_W in solvents containing c M $Fe(ClO_4)_2$ and c M $Fe(ClO_4)_3$. R_{dif} was evaluated by subtraction of R_s and R_{ct} from R_{tot}

Solvent	c (M)	R_{tot} (Ω)	R_s (Ω)	R_{ct} (Ω)	R_{dif} (Ω)	A_W ($\Omega\ s^{-1/2}$)
Water	0.10	351.0	56.0	32.0	263.0	86.2
Water	0.20	236.0	35.4	16.1	184.5	42.8
Water	0.50	65.0	19.8	5.3	39.9	15.7
Water	0.80	42.6	18.1	3.8	20.7	10.8
Water	1.00	39.4	18.1	2.9	18.4	10.0
Water	1.50	28.5	16.3	2.1	10.1	9.1
Water	2.00	27.7	19.6	1.9	6.2	7.0
Water	2.50	37.9	20.0	1.9	16.0	10.4
MeOH	0.05	906.0	221.7	65.2	619.1	176.7
MeOH	0.10	314.0	126.0	22.6	165.4	63.0
MeOH	0.50	95.6	54.6	4.4	36.6	16.2
MeOH	1.00	95.2	60.9	1.8	32.5	9.1
MeOH	1.50	98.2	67.4	1.6	29.2	8.4
MeOH	2.00	110.0	75.5	2.4	32,1	6.8
MeOH	2.50	115.0	83.3	3.2	28.6	7.5
Acetone	0.05	692.0	439.2	35.6	227.2	134.6
Acetone	0.10	333.0	187.0	18.0	128.0	72.0
Acetone	0.20	225.0	130.4	8.6	86.0	29.0
Acetone	0.40	172.0	100.3	5.0	66.7	14.7
Acetone	0.80	192.0	126.8	2.8	62.4	9.0
Acetone	1.00	254.0	160.5	4.5	89.0	9.2
Acetone	1.20	251.0	180.0	4.5	66.5	8.8
PC	0.05	1265.0	726.8	75.6	425.6	255.8
PC	0.10	813.0	615.0	27.0	171.0	70.0
PC	0.20	528.0	387.6	11.5	128.9	31.2
PC	0.50	537.0	447.9	11.4	77.7	17.5
PC	1.00	741.0	663.3	12.9	64.8	15.0
PC	1.50	726.0	674.1	13.2	38.7	13.9

2. In (a) the aqueous solution, R_{tot} decreases from 65.0 Ω at 0.5 M to 28.5 Ω at 1.5 M, and then increases to 37.9 Ω at 2.5 M. The decrease in R_{tot} in the low c region is due to the increase in the number ($\propto c$) of charge carriers, such as Fe^{2+} and Fe^{3+}. This behavior is consistent with the literature.[6] Similar local minima structures in the c–R_{tot} plot are also observed for the MeOH, acetone and PC solutions (Table 2).

Let us estimate the maximum value of ZT in the aqueous electrolyte at 300 K with the use of R_{tot} shown in Table 2. The maximum value of $\sigma\left(=\dfrac{d}{SR_{tpt}}\right)$ is 86.0 mS cm^{-1} at $c = 2.0$ M. Kim *et al.*[6] reported c-dependence of α and κ in an aqueous solution containing $Fe(ClO_4)_2/Fe(ClO_4)_3$. From the extrapolation of the reported data, we evaluated $\alpha = 1.76$ mV K^{-1} and $\kappa = 0.4$ W K^{-1} m^{-1} at 2.0 M. Then, we obtained $ZT = 0.020$ at 2.0 M. The ZT value is smaller than the value ($= 0.036$ (ref. 6) at 0.8 M) reported by Kim *et al.*,[6] reflecting the smaller σ obtained in the present experiment. We note that effective σ of a LTE is influenced by the microscopic structure of the electrodes as well as the convection of the electrolyte.

3.2 Electrochemical impedance spectroscopy

Fig. 2 shows examples of the Cole–Cole plots of complex impedance for several solutions containing dissolved Fe^{2+}/Fe^{3+} at 298 K: (a) water, (b) MeOH, (c) acetone, and (d) PC. The Cole–Cole plot of 0.1 M MeOH solution (Fig. 2(b)) shows a prototypical shape. The plot shows a semicircle on the left side and

a straight line with an inclination of 45° on the right side. The resistances on the left and right sides of the semicircle correspond to R_s and $R_s + R_{ct}$, respectively. The intersection of the

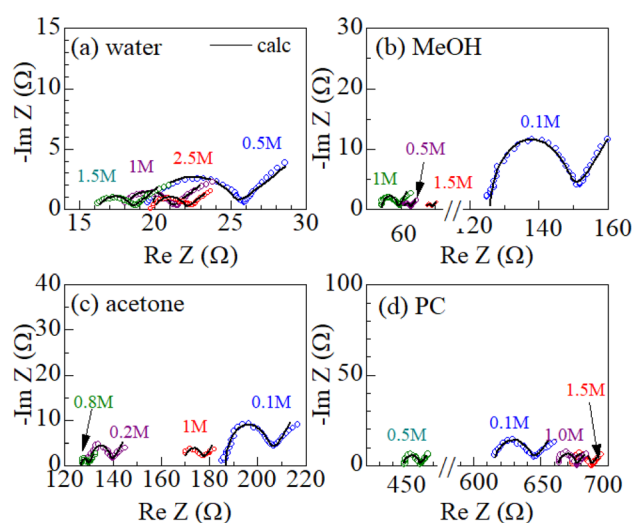**Fig. 2** Cole–Cole plots of complex impedance for several solutions containing dissolved Fe^{2+}/Fe^{3+} at 298 K: (a) water, (b) MeOH, (c) acetone, and (d) PC. The solid curves are the results of least-squares fits with a Randles equivalent circuit composed of R_s, R_{ct}, C_d, and Z_ω (see text).

straight line with the horizontal axis corresponds to $R_s + R_{ct} - 2A_W{}^2 C_d$. Similar behaviors are also observed in the other solutions. The solid curves in Fig. 1 are the results of least-squares fits with a Randles equivalent circuit composed of R_s, R_{ct}, C_d, and Z_ω. The Randles equivalent circuit well reproduces the observed complex impedance. Thus, we obtained R_s, R_{ct}, C_d, and A_W. We further evaluate $R_{dif} (= R_{tot} - R_s - R_{ct})$ with the use of R_{tot}. The obtained R_s, R_{ct}, R_{dif}, and A_W values are listed in Table 2.

A_W is expected to have a strong correlation with R_{dif} because $Z_\omega [= A_W(\omega^{-1/2} - i\omega^{-1/2})]$ describes the diffusion process of the reactants/products. We calculated the correlation coefficient X between A_W and $R_{dif} (= R_{tot} - R_s - R_{ct})$ for each solution system; $X = 0.976$ for water, 0.995 for MeOH, 0.980 for acetone, and 0.988 for PC. The positive correlation ($X \geq 0.976$) between A_W and R_{dif} strongly supports the correctness of our evaluation method of R_{dif}.

3.3 Concentration dependence of resistivity components

Fig. 3 shows the c-dependence of (a) $R_s{}^{-1}$, (b) $R_{ct}{}^{-1}$, (c) $R_{dif}{}^{-1}$, and (d) $R_{tot}{}^{-1}$ in several solutions containing dissolved Fe^{2+}/Fe^{3+} at 298 K. For the convenience of explanation, the horizontal axis is normalized by the critical concentration c^* of each solvent. At $c = c^*$, all solvent molecules are on average coordinated with Fe ions.
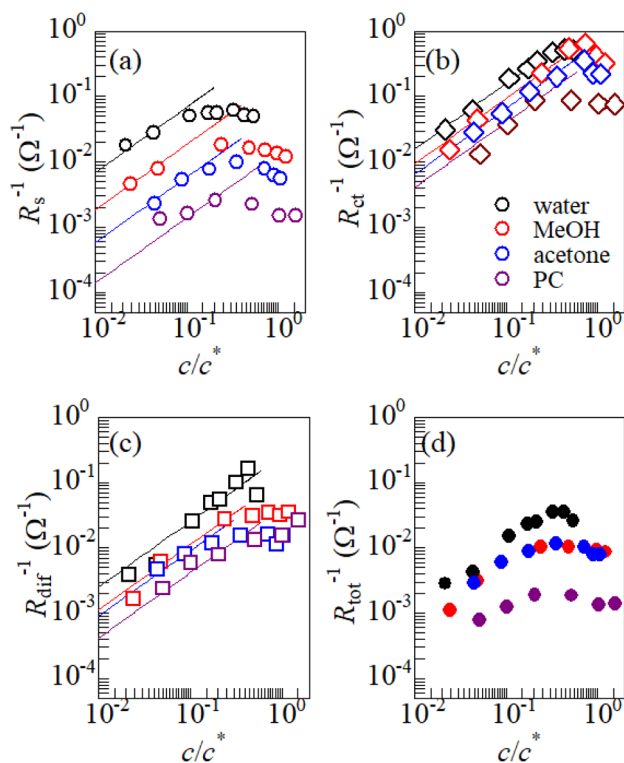

Fig. 3 Solute concentration (c) dependence of (a) $R_s{}^{-1}$, (b) $R_{ct}{}^{-1}$, (c) $R_{dif}{}^{-1}$, and (d) $R_{tot}{}^{-1}$ in several solutions containing dissolved Fe^{2+}/Fe^{3+} at 298 K. The horizontal axis is normalized by the critical concentration c^* of each solvent. The straight lines in (a), (b), and (c) represent the linear relation with $\frac{c}{c^*}$.

First, let us examine the solvent dependence of $R_s{}^{-1}$, $R_{ct}{}^{-1}$, and $R_{dif}{}^{-1}$. Significant solvent dependence is observed for (a) $R_s{}^{-1}$. $R_s{}^{-1}$ values at $\frac{c}{c^*} = 0.1$ are 69.5×10^{-3} Ω^{-1} in water, 17.1×10^{-3} Ω^{-1} in MeOH, 6.7×10^{-3} Ω^{-1} in acetone, and 1.4×10^{-3} Ω^{-1} in PC. The $R_s{}^{-1}$ values in organic solutions are much smaller than those in aqueous solutions. In contrast, $R_{ct}{}^{-1}$ and $R_{dif}{}^{-1}$ have relatively small solvent dependence. In this sense, reducing R_s is effective to reduce R_{tot} in organic solution. Shortening d is especially effective because $\kappa (\approx 0.2$ W K^{-1} m^{-1}) of an organic solvent is much smaller than $\kappa (= 0.6$ W K^{-1} m^{-1}) of water. Reflecting the small κ in organic solvent, a sufficient ΔT is expected between the electrodes, even in the cell with smaller d.

Next, let us investigate the $\frac{c}{c^*}$ dependence of $R_s{}^{-1}$, $R_{ct}{}^{-1}$, and $R_{dif}{}^{-1}$. In the small $\frac{c}{c^*}$ region, $R_s{}^{-1}$ increases linearly with $\frac{c}{c^*}$ as indicated by the straight lines in Fig. 3(a). The increase in $R_s{}^{-1}$ is due to the increase in the number ($\propto c$) of charge carriers, such as Fe^{2+} and Fe^{3+}. Upon further increasing $\frac{c}{c^*}$ beyond ~ 0.3, $R_s{}^{-1}$ begins to decrease with $\frac{c}{c^*}$. Similarly, in the small $\frac{c}{c^*}$ region, $R_{ct}{}^{-1}$ and $R_{dif}{}^{-1}$ increase linearly with $\frac{c}{c^*}$ as indicated by the straight lines in Fig. 3(b) and (c), respectively. The increase in $R_{ct}{}^{-1}$ and $R_{dif}{}^{-1}$ is due to the increase ($\propto c$) of reactant/product concentration, *i.e.*, Fe^{2+}/Fe^{3+}. Upon further increasing $\frac{c}{c^*}$ beyond ~ 0.5, $R_{ct}{}^{-1}$ and $R_{dif}{}^{-1}$ begin to saturate. The saturation of $R_{ct}{}^{-1}$ can be ascribed to the finite reaction number ($N_{reaction}$) per unit time at the electrode surface. The redox reaction cannot keep up with the supply of reactants when the number ($N_{reactant} \propto c$) of reaching reactants per unit time exceeds $N_{reaction}$. In such a region, $N_{reaction}$ becomes the rate-determining factor for the charge-transfer current J_{ct}, and hence, $R_{ct}{}^{-1}$. As a result, R_{ct} becomes constant at sufficiently large c.

4 Discussion

4.1 Concentration dependence of R_s

Now, let us discuss the solution parameters that determine R_s. $R_s{}^{-1} \left(= \frac{s}{d}\sigma_s \right)$ is expressed as $R_s{}^{-1} = \frac{sF}{d}\sum_j |z_j| u_j C_j$,[23] where F, z_j, u_j, and C_j are the Faraday constant, charge number, mobility, and molar concentration of the j-th ion, respectively. By substituting $u_j = \frac{|z_j|e}{6\pi\eta r_j}$, we obtain $R_s{}^{-1} = \frac{sFec}{6\pi d\eta}\sum_j \frac{|z_j|^2}{r_j}$. Note that $C_{Fe^{2+}} = C_{Fe^{3+}} = c$ in the present solutions. By assuming $\sum_j \frac{|z_j|^2}{r_j}$ is independent of c in each solution, we obtain the simple relation $R_s{}^{-1} \propto C_s \frac{c}{\eta}$, where C_s is a constant. The top panels of Fig. 4(a)–(d) show η of each solution against c. The η values were evaluated at 298 K using a sine-wave vibro viscometer (SV-10; A&D Company Limited). In all solutions, η increases nonlinearly with c. The solid curves are the results of least-
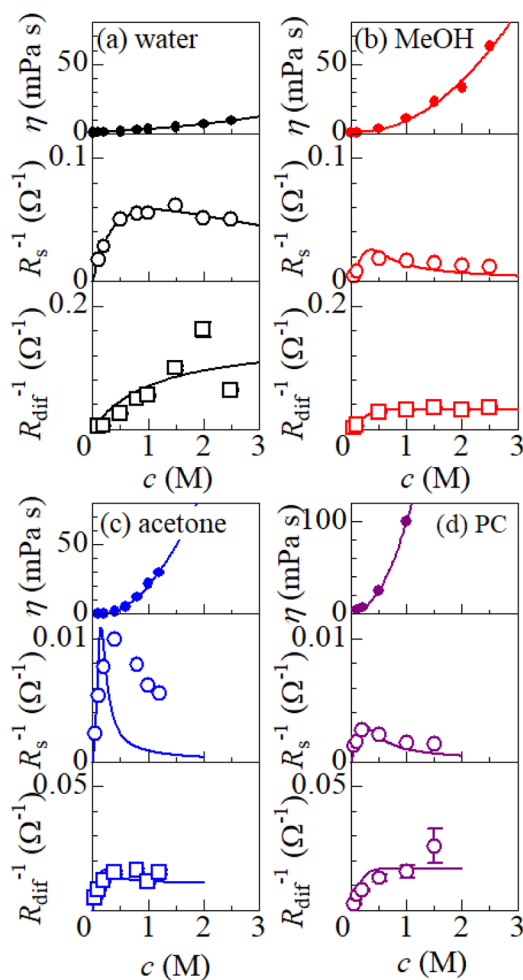
Fig. 4 (a) Viscosity η (top), R_{s}^{-1} (middle), R_{dif}^{-1} (bottom) in aqueous solutions containing dissolved Fe^{2+}/Fe^{3+} at 298 K against solute concentration c. (b) η, R_{s}^{-1}, and R_{dif}^{-1} in MeOH solutions containing dissolved Fe^{2+}/Fe^{3+} at 298 K against c. (c) η, R_{s}^{-1}, and R_{dif}^{-1} in acetone solutions containing dissolved Fe^{2+}/Fe^{3+} at 298 K against c. (d) η, R_{s}^{-1}, and R_{dif}^{-1} in PC solutions containing dissolved Fe^{2+}/Fe^{3+} at 298 K against c. The solid curves in the upper panels are the results of least-squares fits with a quadratic function. The solid curves in the middle panels are the results of least-squares fits with the $\frac{c}{\eta(c)}$ function. The solid curves in the bottom panels are the results of least-squares fits with the $\frac{c}{\eta(c)^{1/2}}$ function.

squares fits with a quadratic function. With use of the quadratic function $\eta(c)$, the empirical formula, $R_{\mathrm{s}}^{-1} = C_{\mathrm{s}} \dfrac{c}{\eta(c)}$, can be calculated.

The middle panels of Fig. 4(a)–(d) show comparisons between observed R_{s}^{-1} (open circles) and empirical formula (solid curves) against c. We note that there is only one fitting parameter (C_{s}) to adjust the magnitude but no parameter to adjust the shape. Nevertheless, the curve reproduces the observed R_{s}^{-1} well, except for (c) acetone solution. In Table 3, we listed C_{s}. Except for the acetone solution, the solvent dependence of C_{s} is rather small, falling between 0.104 mPa s M^{-1} Ω^{-1} and 0.183 mPa s M^{-1} Ω^{-1}. This is probably because the r value does not change greatly depending on the solvent.

Table 3 Coefficients (C_{s} and C_{dif}) of empirical formulas, $R_{\mathrm{s}}^{-1} = C_{\mathrm{s}} \dfrac{c}{\eta(c)}$ and $R_{\mathrm{dif}}^{-1} = C_{\mathrm{dif}} \dfrac{c}{\eta(c)^{1/2}}$, determined by least-squares fits with the observed data. MeOH and PC represent methanol and propylene carbonate, respectively

Solvent	C_{s} (mPa s M^{-1} Ω^{-1})	C_{dif} (mPa$^{1/2}$ s$^{1/2}$ M^{-1} Ω^{-1})
Water	0.183	0.125
MeOH	0.132	0.099
Acetone	0.019	0.053
PC	0.104	0.166

In (c) acetone solution, the shape of the c–R_{s}^{-1} plot (open circles) is qualitatively different from the shape of the empirical formula (solid curve). In the region of $c \geq 0.5$, the empirical formula results decrease steeply while the observed R_{s}^{-1} decreases slowly. If C_{s} is set to $\sim$0.1, the agreement between the calculated and observed values is improved in the region of $c \geq 0.5$ even though the calculated value is much larger in the region of $c \sim 0.3$. This implies that an additional factor, *e.g.*, the repulsive interaction between Fe ions, suppressed R_{s} in the region of $c \sim 0.3$.

4.2 Concentration dependence of R_{dif}

Finally, let us consider the relationship between R_{dif}^{-1} and η. R_{dif}^{-1} is proportional to the diffusion current J_{dif}, which is expressed as $J_{\mathrm{dif}} \propto D \dfrac{\mathrm{d}C}{\mathrm{d}x}$. Replacing the differential with the difference, we get $J_{\mathrm{dif}} \propto \dfrac{D \Delta C}{\Delta x}$,[23] where Δx and ΔC are the diffusion length and concentration difference between electrode surface and bulk solution, respectively. In one-dimensional diffusion, Δx is expressed as $\Delta x = \sqrt{2Dt} \propto D^{1/2}$, where t is the elapsed time. Then, J_{dif} is proportional to $cD^{1/2}$ because $\Delta C \propto c$. From the Stokes–Einstein equation, we obtain $D = \dfrac{k_{\mathrm{B}}T}{6\pi\eta r}$. Finally, we obtain an empirical relation $R_{\mathrm{dif}}^{-1} = C_{\mathrm{dif}} \dfrac{c}{\eta(c)^{1/2}}$, where C_{dif} is a constant. We can calculate the empirical formula with use of the quadratic function $\eta(c)$.

The bottom panels of Fig. 4(a)–(d) show comparisons between the observed R_{dif}^{-1} (open circles) and empirical formula (solid curves) against c. We note that there is only one fitting parameter (C_{dif}) to adjust the magnitude. Nevertheless, the curve reproduces the observed R_{dif}^{-1} well. In Table 3, we list the C_{dif} values. The solvent dependence of C_{dif} is rather small, falling between 0.053 mPa$^{1/2}$ s$^{1/2}$ M^{-1} Ω^{-1} and 0.166 mPa$^{1/2}$ s$^{1/2}$ M^{-1} Ω^{-1}. This is probably because the r value does not change greatly depending on the solvent.

5 Conclusions

In conclusion, we investigated the c-dependence of R_{s}, R_{ct}, and R_{dif} in dissolved-Fe^{2+}/Fe^{3+}-containing aqueous, MeOH, acetone, and PC solutions. We found that the c-dependence of R_{s} and R_{dif} is well reproduced by the empirical formulas $R_{\mathrm{s}}^{-1} = C_{\mathrm{s}} \dfrac{c}{\eta(c)}$ and

$R_{dif}^{-1} = C_{dif} \dfrac{c}{\eta(c)^{1/2}}$. We further found that the magnitudes of C_s and C_{dif} are nearly independent of the solvent, suggesting that η is one of the significant solution parameters that determine R_s and R_{dif}. Our findings suggest that σ of the electrolyte solution can be increased through reducing η.

Author contributions

Dai Inoue: data curation, formal analysis, and investigation. Yutaka Moritomo: conceptualization, supervision, writing – original draft, and writing – review & editing.

Conflicts of interest

There are no conflicts to declare.

Acknowledgements

Notes and references

1 Q. Long, G. Jiang, J. Zhou, D. Zhao, P. Jia and S. Nie, *Nano Energy*, 2024, **120**, 109130.

2 T. Ikeshoji, *Bull. Chem. Soc. Jpn.*, 1987, **60**, 1505; I. Quickenden and Y. Mua, *J. Electrochem. Soc.*, 1995, **142**, 3985; Y. Mua and T. I. Quickenden, *J. Electrochem. Soc.*, 1996, **143**, 2558; J. Kawamura, M. Shimoji and H. Hoshino, *J. Phys. Soc. Jpn.*, 1981, **50**, 194; A. Schiraldi, E. Pezzati and P. Baldini, *J. Phys. Chem.*, 1985, **89**, 1528; R. Hu, B. A. Cola, N. Haram, J. N. Barisci, S. Lee, S. Stoughton, G. Wallace, C. Too, M. Thomas, A. Gestos, M. Ed Cruz, J. P. Ferraris, A. A. Zakhidov and R. H. Baughman, *Nano Lett.*, 2010, **10**, 838; D. R. MacFarlane, N. Tachikawa, M. Forsyth, J. M. Pringle, P. C. Howlett, G. D. Elliott, J. F. Davis Jr, M. Watanabe, P. Simon and C. A. Angell, *Energy Environ. Sci.*, 2014, **7**, 232; M. Bonetti, S. Nakamae, M. Roger and P. Guenoun, *J. Chem. Phys.*, 2011, **134**, 114513; T. J. Abraham, D. R. MacFarlane and J. M. Pringle, *Chem. Commun.*, 2011, **47**, 6260; M. Romano, S. Gambhir, J. Razal, A. Gestos, G. Wallace, J. Chen and J. Therm, *J. Therm. Anal. Calorim.*, 2012, **109**, 1229; M. S. Romano, N. Li, D. Antiohos, J. M. Razal, A. Nattestad, S. Beirne, S. Fang, Y. Chen, R. Jalili, G. G. Wallace, R. Baughman and J. Chen, *Adv. Mater.*, 2013, **25**, 6602; T. J. Abraham, D. R. MacFarlane and J. M. Pringle, *Energy Environ. Sci.*, 2013, **6**, 2639; A. Gunawan, C.-H. Lin, D. A. Buttry, V. Mujica, R. A. Taylor, R. S. Prasher and P. E. Phelan, *Nanoscale Microscale Thermophys. Eng.*, 2013, **17**, 304; N. Jiao, T. J. Abraham, D. R. MacFarlane and J. M. Pringle, *J. Electrochem. Soc.*, 2014, **161**, D3061; S. Uhl, E. Laux, T. Journot, L. Jeandupeux, J. Charmet and H. Keppner, *J. Electron. Mater.*, 2014, **43**, 3758; A. Gunawan, H. Li, C.-H. Lin, D. A. Buttry, V. Mujica, R. A. Taylor, R. S. Prasher and P. E. Phelan, *Int. J. Heat Mass Transfer*, 2014, **78**, 423; M. A. Lazar, D. Al-Masri, D. R. MacFarlane and J. M. Pringle, *Phys. Chem. Chem. Phys.*, 2016, **18**, 1404.

3 Y. Liang, J. K.-H. Hui, M. Morikawa, H. Inoue, T. Yamada and N. Kimizuka, *ACS Appl. Energy Mater.*, 2021, **4**, 5326.

4 B. Yu, J. Duan, H. Cong, W. Xie, R. Liu, X. Ahuang, H. Wang, B. Qi, M. Xu and L. Wan, *Science*, 2020, **370**, 342.

5 Y. Xaing, X. Guo, H. Zhu, Q. Zhang and S. Zhu, *Chem. Eng. J.*, 2023, **461**, 142018.

6 J. H. Kim, J. H. Lee, E. E. Palen, M.-S. Suh, H. H. Lee and R. J. Kang, *Sci. Rep.*, 2019, **9**, 8706.

7 M. A. Buckingham, F. Marken and L. Aldous, *Sustainable Energy Fuels*, 2018, **2**, 2717.

8 J. Duan, G. Feng, B. Yu, J. Li, M. Chen, P. Yang, J. Feng, K. Liu and J. Zhou, *Nat. Commun.*, 2018, **9**, 5146.

9 T. Kim, J. S. Lee, G. Lee, H. Yoon, J. Yoon, T. J. Kangd and Y. H. Kim, *Nano Energy*, 2017, **31**, 160.

10 M. Sindhuja, B. Lohith, V. Sudha, G. R. Manjunath and S. Harinipriya, *Mater. Res. Express*, 2017, **4**, 075513.

11 H. Im, T. Kim, H. Song, J. Choi, J. S. Park, R. Ovalle-Robles, H. D. Yang, K. D. Kihm, R. H. Baughman, H. H. Lee, T. J. Kang and Y. H. Kim, *Nat. Commun.*, 2016, **7**, 10600.

12 H. Zhou, T. Yamada and N. Kimizuka, *J. Am. Chem. Soc.*, 2016, **138**, 10502.

13 A. H. Kazim and B. A. Cola, *J. Electrochem. Soc.*, 2016, **163**, F867.

14 S. W. Lee, Y. Yang, H.-W. Lee, H. Ghasemi, D. Kraemer, G. Chen and Y. Cui, *Nat. Commun.*, 2014, **5**, 3942.

15 Y. Tanaka, A. Wake, D. Inoue and Y. Moritomo, *Jpn. J. Appl. Phys.*, 2024, **63**, 014002.

16 S.-M. Jung, S.-Y. Kang, B.-J. Lee, J. Kwon, D. Lee and Y.-T. Kim, *Adv. Funct. Mater.*, 2023, **33**, 2304067.

17 B. Yu, H. Xiao, Y. Zeng, S. Liu, D. Wu, P. Liu, J. Guo, W. Xie, J. Duan and J. Zhou, *Nano Energy*, 2022, **93**, 106795.

18 A. Wake, D. Inoue and Y. Moritomo, *Appl. Phys. Express*, 2022, **15**, 054002.

19 A. Wake, D. Inoue and Y. Moritomo, *Jpn. J. Appl. Phys.*, 2023, **62**, 014002.

20 J. Duan, B. Yu, L. Huang, B. Hu, M. Xu, G. Feng and J. Zhou, *Joule*, 2021, **5**, 768.

21 S. W. Angrist, *Direct Energy Conversion*, Allyn and Bacon, Inc., Boston, 1982.

22 D. Inoue, H. Niwa, H. Nitani and Y. Moritomo, *J. Phys. Soc. Jpn.*, 2021, **90**, 033602.

23 A. J. Bard, L. R. Faulkner, and H. S. White, *Electrochemical Methods*, Wiley, West Sussex, 2022.

24 Y. Fukuzumi, Y. Hinuma and Y. Moritomo, *Jpn. J. Appl. Phys.*, 2019, **58**, 065501.